CHEMISTRY OF MATERIALS

pubs.acs.org/cm

Article

ZrO_2 Monolayer as a Removable Etch Stop Layer for Thermal Al_2O_3 Atomic Layer Etching Using Hydrogen Fluoride and Trimethylaluminum

David R. Zywotko, Omid Zandi, Jacques Faguet, Paul R. Abel, and Steven M. George*

Cite This: *Chem. Mater.* 2020, 32, 10055−10065

Read Online

ACCESS | Metrics & More | Article Recommendations

ABSTRACT: A ZrO_2 monolayer was demonstrated as a removable etch stop layer (ESL) for thermal Al_2O_3 atomic layer etching (ALE) using HF and $Al(CH_3)_3$ (trimethylaluminum (TMA)) as the reactants. The ZrO_2 ESL was deposited on Al_2O_3 using tetrakis(ethylmethylamido)zirconium (TEMAZ) and H_2O. *In situ* quartz crystal microbalance (QCM) measurements showed that a ZrO_2 coverage of ~190 ng/cm^2 completely blocked thermal Al_2O_3 ALE at 285 °C. This ZrO_2 coverage is equivalent to approximately one ZrO_2 monolayer. The inhibition of the Al_2O_3 etch rate was proportional to the ZrO_2 fractional coverage. The ZrO_2 ESL was effective for hundreds of thermal Al_2O_3 ALE cycles. In terms of the surface chemistry, the ZrO_2 ESL is known to be fluorinated to a ZrO_xF_y or ZrF_4 layer by HF exposure. This fluorinated layer restricts etching by preventing the ligand-exchange reaction with TMA. The fluorinated layer could be easily removed using thermal ALE with HF and $AlCl(CH_3)_2$ (dimethylaluminum chloride (DMAC)) as the reactants. The ZrO_2 ESL could be deposited and removed repeatedly without changing the Al_2O_3 etch rate. X-ray photoelectron spectroscopy (XPS) studies observed no trace of Zr on the Al_2O_3 surface after 7−8 cycles of HF and DMAC sequential exposures. Area selective deposition of the ZrO_2 ESL would lead to area selective etching using HF and TMA as the reactants.

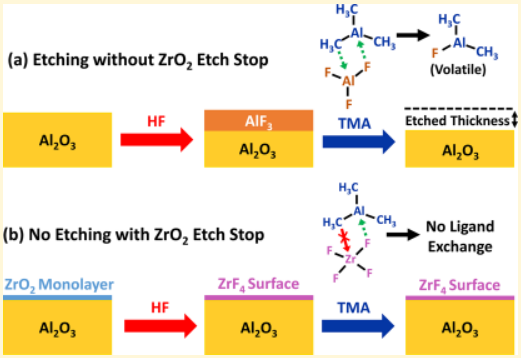

1. INTRODUCTION

Continued miniaturization of devices has created the need for atomic layer control of processing. Atomic layer deposition (ALD) and atomic layer etching (ALE) methods have responded to this challenge. ALD and ALE are both based on sequential, self-limiting surface reactions.[1,2] For ALE, these reactions involve self-limiting surface modification and volatile release.[2−4] ALE can be accomplished using plasma ALE where energetic ions or neutrals release the modified surface material.[2,5] ALE can also be achieved by thermal ALE where the modified surface material is released by thermal reactions.[3,4,6]

Thermal atomic layer etching (ALE) has been demonstrated for many materials including Al_2O_3,[3,7,8] HfO_2,[8−10] ZrO_2,[8] ZnO,[11] TiN,[12] W,[13] Si,[14] SiO_2,[15] and Si_3N_4.[16] One of the main mechanisms of thermal ALE is fluorination and ligand-exchange.[3,4,6] For example, thermal Al_2O_3 ALE can be accomplished using HF and $Al(CH_3)_3$ (trimethylaluminum (TMA)) as the reactants.[7] During thermal Al_2O_3 ALE, the Al_2O_3 surface is first fluorinated by HF exposure to form an AlF_xO_y or AlF_3 surface layer.[7,17,18] During the subsequent TMA exposure, a ligand-exchange transmetalation reaction with the fluorinated surface layer creates volatile etching products.[7,19,20] Al_2O_3 etch rates of 0.14−0.75 Å/cycle are observed at temperatures from 250 to 325 °C.[7]

Future semiconductor fabrication will increasingly occur beyond the limits of photolithography and will require maskless, bottom-up processing.[21,22] Selectivity will be required in both deposition and etching during device fabrication.[22,23] The chemistry of thermal ALE has been shown to be very selective.[10,12,24] This selectivity results primarily from the ligand-exchange reaction during thermal ALE.[24] Selectivity is derived from the requirement that the products from the ligand-exchange reaction need to be both stable and volatile. In addition, there is a need for even greater selectivity during thermal ALE beyond the inherent selectivity from the ligand-exchange reactions to meet a wide range of processing challenges.

More selectivity in thermal ALE could result from the development of an etch stop layer (ESL). An ESL serves to

Received: August 14, 2020
Revised: November 13, 2020
Published: November 29, 2020

https://dx.doi.org/10.1021/acs.chemmater.0c03335
Chem. Mater. 2020, 32, 10055−10065

stop an etch process at a desired interface or to protect a surface from etching during device processing.[21,25] Typically, an ESL is utilized to inhibit aggressive etching involving plasmas or corrosive chemicals. An ESL of sufficient thickness is usually required to withstand the physical damage resulting from plasma processing. An ESL can also be employed to emit detectable signals that determine the time to stop etching.[26]

Device miniaturization is leaving very little room for extra layers employed to facilitate processing such as ESLs.[27] As critical dimensions are reduced to <10 nm in advanced architectures, the necessary thickness of the ESL must be extremely thin. The ultimate ultrathin ESL would be an atomically thick layer or monolayer. Ideally, this monolayer ESL would also have the ability to be deposited selectively on particular materials to obtain selective thermal ALE of one material in the presence of other neighboring materials.

In this work, *in situ* quartz crystal microbalance (QCM) studies were performed to define an ultrathin ESL that is effective at inhibiting thermal ALE. The ESL was explored using ZrO_2 ALD to inhibit thermal Al_2O_3 ALE using HF and TMA as the reactants. The ZrO_2 surface layer is fluorinated to ZrO_xF_y or ZrF_4 by exposure to HF.[28] When exposed to the subsequent TMA dose, this fluorinated Zr layer does not undergo ligand-exchange with TMA.[24] Because there are no volatile products released, the underlying Al_2O_3 substrate should be protected from etching. Repeated sequential exposures of HF and TMA should then result in no change in the Al_2O_3 substrate covered with the ZrO_2 ESL.

The *in situ* QCM investigations also attempted to measure the minimum effective film thickness to achieve complete blocking of thermal Al_2O_3 ALE. The ZrO_2 ESL may reduce the thermal Al_2O_3 ALE progressively as a function of ZrO_2 fractional coverage. An ideal ESL would display the complete blocking of thermal Al_2O_3 ALE at a ZrO_2 coverage of one monolayer. Experiments also tested the effectiveness of the ZrO_2 ESL versus number of thermal Al_2O_3 ALE cycles. The goal for an ideal ZrO_2 ESL would be the repeated application and removal of the ESL from the Al_2O_3 substrate without any effect on the Al_2O_3 etch rate after removing the ESL.

2. EXPERIMENTAL SECTION

2.A. Hot-Wall Viscous Flow Reactor with *in Situ* Quartz Crystal Microbalance. These ESL studies were performed in a viscous-flow hot-wall reaction chamber.[29] The main reaction chamber was a 316-grade stainless steel flow tube measuring 30 cm in length. The custom reactor was assembled in-house to prioritize low-noise quartz crystal microbalance (QCM) measurements and ideal flow conditions.[29] These ideal conditions were achieved by incorporating a 15 cm preheat zone to allow process gases to mix and thermally equilibrate before reaching the QCM surface.[30]

The reaction chamber was equipped with a chemical series dual-stage rotary vane pump (Pascal 2010C1, Pfeiffer). The pressure was monitored by two capacitance manometers with measurement ranges of 10 Torr (Baratron 121A, MKS) and 1000 Torr (Baratron 623F, MKS). The pump maintained a chamber base pressure of ~20 mTorr without any process gas flow.

An *in situ* quartz crystal microbalance (QCM) was mounted within the isothermal region of the reactor flow tube. The QCM monitored the mass changes while precursors were exposed to the QCM surface. The *in situ* QCM unit (CDS-A0E47, Inficon) was modified for use in a gas-phase deposition system. The modification was accomplished by sealing the unit with a low-outgassing, high temperature epoxy (Epo-Tek H21D, Epoxy Technology Inc.) and converting the water-cooling system into a backside gas purge. These steps prevented backside film deposition and corrosion of the internal electrical components.[29] The QCM crystal (gold coated, 6 MHz, 285 °C optimized, Inficon) changed resonance frequency when mass was added or removed from the QCM surface. This QCM crystal paired with a thin film deposition monitor (Maxtek TM-400, Inficon) converted the frequency change into a change of mass with a mass resolution of ~0.375 ng/cm^2.

During normal operation, a constant flow of high purity argon (Prepurified, 99.998%, Airgas) at 220 sccm was maintained by three mass-flow controllers. Two mass-flow controllers (type 1179A, MKS) were positioned upstream of the main chamber and were dedicated to the two precursors. Each controller streamed 100 sccm of Ar gas. This Ar gas flow served as a precursor carrier and purge gas in the reaction chamber. The third mass-flow controller (type 1159B, MKS) maintained an Ar gas flow at 20 sccm to purge the backside of the QCM crystal before exiting downstream of the active sensor area.[29] The combined Ar flow of 220 sccm produced an experimental base pressure of ~1.8 Torr in the reactor.

The reactor wall temperature was maintained by two insulating ceramic fiber heaters (VS102A06S, Watlow) that encased the reactor body. The heaters were controlled using a proportional-integral-derivative (PID) temperature controller (2408, Eurotherm) and corresponding power controller (7100A, Eurotherm). The combination of insulating heaters and PID controllers maintained the reactor temperature within ±0.1 °C of the set point. The upstream preheat zone used similar ceramic fiber heaters (VS102A12S, Watlow) and an identical PID system. The preheat zone thermally equilibrated the process gases to the reaction temperature before reaching the QCM mass sensor. The preheating treatment prevents inaccurate mass readings and misleading frequency drifting.[30] The QCM system was allowed a minimum of 24 h to thermally equilibrate with the reactor after installation.

2.B. Film Deposition and Etching. To prevent damage from corrosion, the reactor walls and QCM system were passivated with an Al_2O_3 ALD film thickness of 50 nm prior to performing any chemistries involving HF. All growth and etching studies were conducted at 285 °C for optimal QCM sensor crystal stability. This temperature is suited well for Al_2O_3 and ZrO_2 ALD and ALE.[7,8,31,32]

Prior to each study, fresh substrate films were grown on the QCM surface. The Al_2O_3 ALD films were grown using trimethylaluminum (TMA, 97%, Sigma-Aldrich) and H_2O (HPLC grade, submicrometer filtered, Fisher Scientific).[32] The Al_2O_3 ALD films were grown using a pulse sequence of TMA dose for 1 s, N_2 purge for 40 s, H_2O exposure for 1 s, and N_2 purge for 40 s. The TMA was contained in a metal Sure/Pac cylinder (Aldrich), and the H_2O was housed in a glass bubbler with an Ultra-Torr fitting (Swagelok). The ZrO_2 ALD films were grown using tetrakis(ethylmethylamido)zirconium(IV) (TEMAZ, 99.99%, Sigma-Aldrich) housed in a stainless-steel bubbler and H_2O.[31] The ZrO_2 ALD films were grown using a pulse sequence of TEMAZ dose for 0.3 s, N_2 purge for 40 s, H_2O exposure for 1 s, and N_2 purge for 40 s. The TMA and H_2O were kept at room temperature, while the TEMAZ bubbler was maintained at 110 °C.

The Al_2O_3 and ZrO_2 ALE experiments used sequential exposures of either TMA or DMAC (97%, Sigma-Aldrich) as the organometallic precursor, and HF vapor derived from an HF−pyridine solution (70 wt % HF, Sigma-Aldrich).[7,8] The pulse sequence during Al_2O_3 ALE using HF and TMA as the reactants was HF dose for 1 s, N_2 purge for 40 s, TMA exposure for 2 s, and N_2 purge for 40 s. The pulse sequence during Al_2O_3 ALE and ZrO_2 ALE using HF and DMAC as the reactants was HF dose for 1 s, N_2 purge for 40 s, DMAC exposure for 2 s, and N_2 purge for 40 s. The DMAC was housed in a Sure/Pac cylinder (Aldrich) and kept at room temperature. The HF−pyridine solution was maintained at room temperature and housed in a gold-coated stainless-steel bubbler to prevent corrosion. The 70% HF-by-weight solution is a convenient source of HF that has a vapor pressure of 90−100 Torr at room temperature with negligible traces of pyridine.[9,33] The TMA, DMAC, and HF exposures produced partial pressure transients of 40 mTorr, 40 mTorr, and 80 mTorr, respectively, over the reactor base pressure of ~1.8 Torr.

The TEMAZ and HF−pyridine were transferred to their custom bubbler vessels in dry N_2-filled glovebags and underwent freeze−

https://dx.doi.org/10.1021/acs.chemmater.0c03335
Chem. Mater. 2020, 32, 10055−10065

pump−thaw cycles to eliminate dissolved gases. All of the precursor doses were controlled by two pneumatically actuated valves (SS-HBVVCR4-C, Swagelok) in combination with a metering valve (SS-4BMRG-VCR, Swagelok). Heating of the additional reactor components and TEMAZ was accomplished using fiberglass-insulating heat tapes (FGH101-080, Omegalux).

2.C. *Ex Situ* Spectroscopic Ellipsometry and X-ray Photoelectron Spectroscopy. Coupons measuring 2 cm × 2 cm were cut from 125 mm boron-doped Si wafers (p-type, ⟨100⟩, Silicon Valley Microelectronics) for *ex situ* studies. The coupons were cleaned with deionized water and methanol and then blown dry with UHP N_2. The samples were allowed to thermally equilibrate in the chamber for a minimum of 2 h prior to beginning the ALD and ALE studies. Al_2O_3 ALD films were grown on the wafers using 50 cycles of Al_2O_3 ALD with TMA and H_2O at 285 °C. The Al_2O_3 film thicknesses were determined by *ex situ* spectroscopic ellipsometry. The samples were then blown with N_2 and reinserted in the chamber for ALE studies.

Ellipsometry measurements were recorded by a spectroscopic ellipsometer (M-200UI, J. A. Woollam) using a 245−1690 nm range and an incidence angle of 70°. The ellipsometer determined the film thickness after the ALD and ALE processes. The collected data were analyzed using the CompleteEASE software from J. A. Woollam Co. The software determined the film thickness by fitting the amplitude ratio (ψ) and phase difference (Δ) based on a supplied Al_2O_3 model.

X-ray photoelectron spectroscopy (XPS) measurements were performed to determine the Zr surface residue after removal of the ESL. Surface survey scans were performed by an X-ray photoelectron spectrometer (PHI 5600) utilizing monochromatic Al Kα radiation (E = 1486 eV). The data were collected with AugerScan (RBD Instruments) and analyzed by CASA XPS software (Casa Software Ltd.).

3. RESULTS AND DISCUSSION

3.A. Demonstration of ZrO_2 Etch Stop Layer (ESL). Initial experiments demonstrated that sequential exposures of HF and TMA are not able to etch ZrO_2 ALD films.[24] For this demonstration, thin ZrO_2 ALD films were deposited for *in situ* quartz crystal microbalance studies at 285 °C. The ZrO_2 films were grown on Al_2O_3 ALD films. The Al_2O_3 ALD films had a thickness of ∼5 nm and the Al_2O_3 ALD film growth ended with a H_2O exposure. The ZrO_2 ALD was performed using sequential exposures of tetrakis(ethylmethylamido)zirconium-(IV) and H_2O. Figure 1 shows the QCM mass change for six cycles of ZrO_2 ALD on the Al_2O_3 film followed by sequential exposures of HF and TMA at 285 °C.

The ZrO_2 ALD film was deposited with an average growth rate of 34 ng/(cm^2 cycle). The first few ZrO_2 ALD cycles on the Al_2O_3 ALD film have a slightly larger growth rate. The six cycles of ZrO_2 ALD shown in Figure 1 deposited ∼220 ng/cm^2 of ZrO_2 on the surface. This mass of ZrO_2 corresponds to a thickness of 3.87 Å based on a ZrO_2 film density of 5.68 g/cm^3.[34] Subsequently, sequential exposures of HF and TMA were applied to the ZrO_2 ALD film at partial pressures of 80 mTorr and 40 mTorr, respectively. The HF and TMA cycles were performed using a timing sequence of 1−40−2−40. This timing sequence denotes an HF exposure of 1 s, a nitrogen purge of 40 s, a TMA exposure of 2 s, and last a nitrogen purge of 40 s.

Figure 1 shows that the sequential HF and TMA exposures on the ZrO_2 ALD film produce repeating mass gains and mass losses. The mass increases during the HF exposure and decreases during the TMA exposure. However, there is no net mass change and no net etching of the ZrO_2 film. In contrast, many other metal oxide films, such as Al_2O_3, will form volatile species when exposed to sequential HF and TMA exposures.[7,19] These results indicate that the ZrO_2 ALD film serves as an ESL for the underlying Al_2O_3 film.

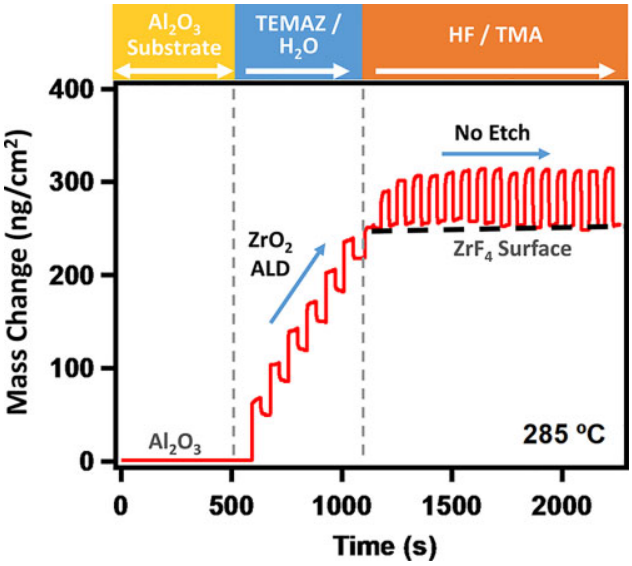

Figure 1. Mass change versus time for ZrO_2 ALD using sequential exposures of TEMAZ and H_2O on Al_2O_3 substrate, followed by sequential exposures of HF and TMA on ZrO_2 ALD film.

To demonstrate that the sequential HF and TMA exposures can etch Al_2O_3, Figure 2 shows results for Al_2O_3 ALE prior to ZrO_2 ALD. The Al_2O_3 film is etched progressively by sequential HF and TMA exposures at a mass change per cycle of 14.5 ng/(cm^2 cycle). This mass change per cycle is equivalent to an etch rate of 0.37 Å/cycle. At approximately 1400 s, ZrO_2 ALD is performed using TEMAZ and H_2O. Following the TMA exposure during Al_2O_3 ALE, a mass of 205 ng/cm^2 of ZrO_2 or 3.61 Å of ZrO_2 is deposited after eight ZrO_2 ALD cycles.

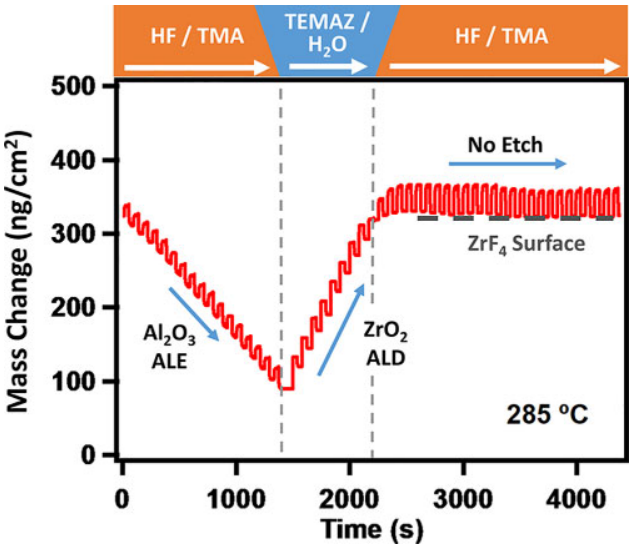

Figure 2. Mass change versus time for Al_2O_3 ALE using sequential exposures of HF and TMA, followed by ZrO_2 ALD using sequential exposures of TEMAZ and H_2O (∼200 ng/cm^2 total), and last, sequential exposures of HF and TMA.

https://dx.doi.org/10.1021/acs.chemmater.0c03335
Chem. Mater. 2020, 32, 10055−10065

The slightly larger number of ZrO_2 ALD cycles required to form a ZrO_2 monolayer in Figure 2 compared with Figure 1 is attributed primarily to differences between the initial surfaces. In Figure 1, the ZrO_2 ALD layer is grown on a hydroxylated Al_2O_3 ALD surface after the H_2O reaction. In Figure 2, the ZrO_2 ALD layer is grown on the surface left after the TMA exposure during Al_2O_3 ALE. The variation between the ZrO_2 ALD nucleation on these different initial surfaces likely affects the ZrO_2 ALD growth rate. In addition, other factors could also influence the ZrO_2 ALD nucleation such as precursor pressure and precursor aging. The TEMAZ precursor slowly decomposed at its 100 °C reservoir temperature. The TEMAZ pressure transients during ZrO_2 ALD varied between 10 and 20 mTorr.

After the ZrO_2 ALD, sequential exposures of HF and TMA are again applied to the ZrO_2 ALD layer on the Al_2O_3 film. Figure 2 shows that there is no etching of the film after ZrO_2 ALD. The mass is constant over multiple HF and TMA exposures. The ZrO_2 ALD film is an ESL for sequential exposures of HF and TMA.

Additional experiments quantified how much ZrO_2 was needed to block the etching of the Al_2O_3 film. Figure 3 displays

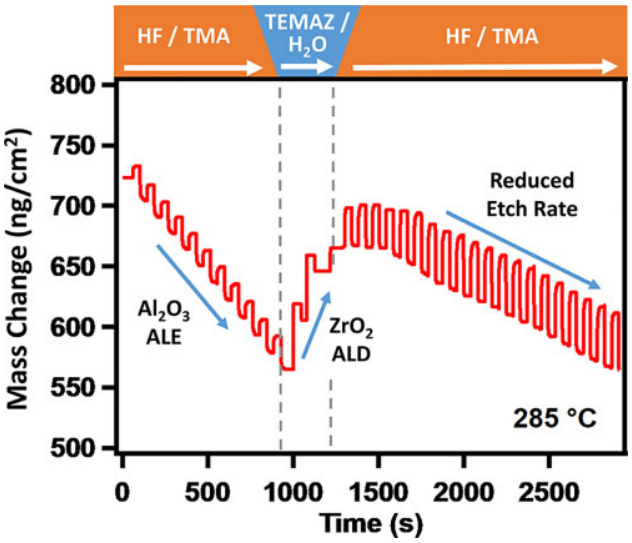

Figure 3. Mass change versus time for Al_2O_3 ALE using sequential exposures of HF and TMA, followed by ZrO_2 ALD using sequential exposures of TEMAZ and H_2O (~90 ng/cm^2 total), and last, sequential exposures of HF and TMA.

mass changes versus time during a similar experiment to the experiment shown in Figure 2. However, only two cycles of ZrO_2 ALD were used to deposit the ZrO_2 layer. These two cycles deposit 81 ng/cm^2 or 1.43 Å of ZrO_2. For this case, the Al_2O_3 ALE is not completely stopped by the ZrO_2 deposition. The Al_2O_3 etching proceeds at an etch rate of 7.2 ng/(cm^2 cycle). This etch rate is a 50% reduction from the normal Al_2O_3 etch rate of 14.5 ng/(cm^2 cycle). This reduction suggests that there is a minimum amount of ZrO_2 deposition that is needed to fully inhibit the Al_2O_3 etching.

To determine the dependence between the Al_2O_3 etch rate and the ZrO_2 mass deposited as an etch stop layer, more experiments were performed with different amounts of deposited ZrO_2. The summary of these results is given in Figure 4. The Al_2O_3 etch rate decreases linearly versus increasing deposited ZrO_2 mass. The Al_2O_3 etch rate

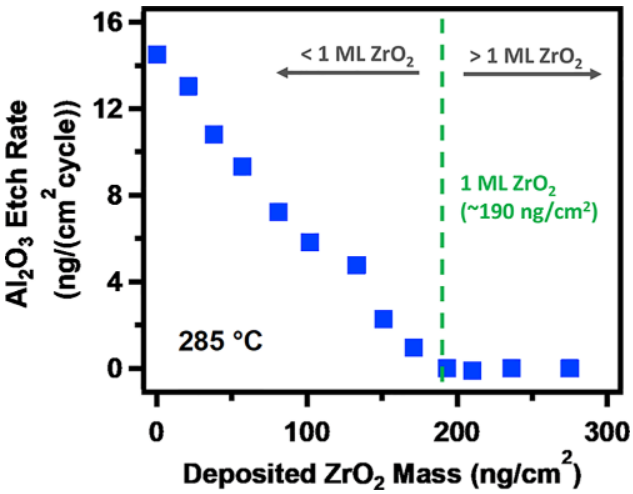

Figure 4. Etch rate of underlying Al_2O_3 film using sequential exposures of HF and TMA versus mass of ZrO_2 overlayer film. Dashed line indicates mass of one complete ZrO_2 monolayer (ML) on Al_2O_3 surface.

approaches zero when the deposited ZrO_2 mass reaches 190 ng/cm^2 or 3.35 Å of ZrO_2. This ZrO_2 mass per area can be used to estimate the ZrO_2 coverage.

The density of ZrO_2 is 5.68 g/cm^3.[34] This mass density is equivalent to a number density of $\rho = 2.78 \times 10^{22}$ ZrO_2 units/cm^3. Assuming that the ZrO_2 units in the ZrO_2 film form a square lattice, the number density can be used to estimate the coverage of ZrO_2 units on the surface as $\rho^{2/3} = 9.2 \times 10^{14}$/cm^2. In addition, the linear density of ZrO_2 units is $\rho^{1/3} = 3.0 \times 10^7$/cm. Likewise, the thickness of one layer of ZrO_2 units is $\rho^{-1/3} = 3.3 \times 10^{-8}$ cm or 3.3 Å. By use of the mass density of ZrO_2 of 5.68 g/cm^3, this thickness of one layer of ZrO_2 units is equivalent to a mass of 188 ng/cm^2.

The results in Figure 4 reveal that the Al_2O_3 etch is stopped at a deposited ZrO_2 mass of ~190 ng/cm^2. This deposited mass is nearly equivalent to the estimate for one monolayer of ZrO_2 units. Prior to reaching a deposited ZrO_2 mass of ~190 ng/cm^2, the inhibition of the Al_2O_3 etch rate is proportional to the ZrO_2 fractional coverage. No ALE of the underlying film is observed when the mass of the ZrO_2 overlayer is greater than or equal to the mass of ~190 ng/cm^2 or one monolayer of ZrO_2 units.

Figure 5 uses the results in Figure 4 to obtain the percentage of Al_2O_3 etch inhibition versus deposited ZrO_2 mass. The deposited ZrO_2 mass is given as a percentage of one ZrO_2 monolayer of 190 ng/cm^2. For example, if 75% of the mass of a ZrO_2 ML or 142 ng is deposited, then the Al_2O_3 etch proceeds at ~25% the normal rate, or about 75% etch inhibition. The correlation between the Al_2O_3 ALE inhibition and the deposited ZrO_2 is linear. This linear relationship suggests that the Al_2O_3 ALE is blocked at every surface location covered by a ZrO_2 unit.

The schematic in Figure 6 depicts the surface chemistry that occurs during sequential HF and TMA exposures on clean Al_2O_3 films and ZrO_2-covered Al_2O_3 films. Both the Al_2O_3 and ZrO_2 surfaces are fluorinated by HF exposure and form AlF_3 and ZrF_4, respectively.[17,18,28] The fluorination reactions are thermochemically favorable with negative standard free energy changes at 285 °C and proceed as[35]

https://dx.doi.org/10.1021/acs.chemmater.0c03335
Chem. Mater. 2020, 32, 10055−10065

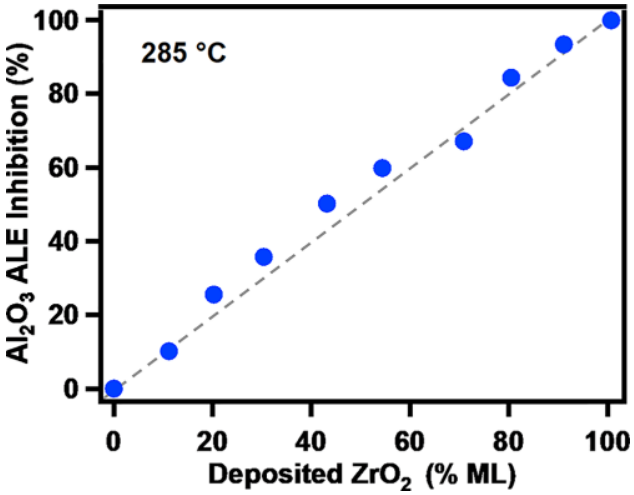

Figure 5. Percentage of Al_2O_3 ALE inhibition versus amount of ZrO_2 deposited as percentage of one ZrO_2 monolayer.

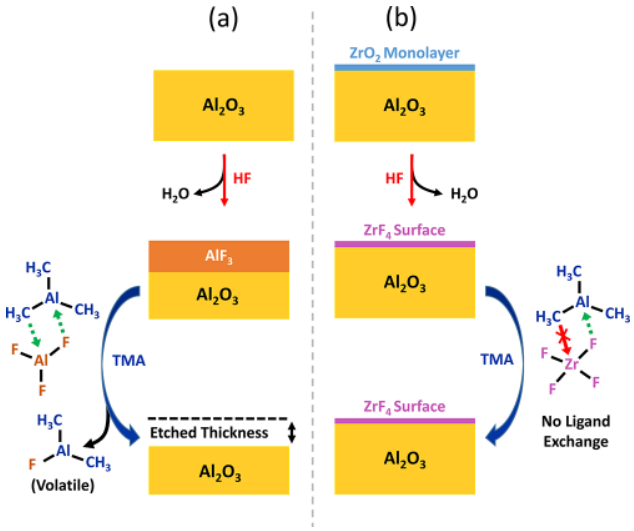

Figure 6. Schematic of etch stop layer mechanism on (a) uncoated Al_2O_3 and (b) ZrO_2-coated Al_2O_3. HF exposure fluorinates both uncoated Al_2O_3 and ZrO_2-coated Al_2O_3 and forms AlF_3 and ZrF_4, respectively. (a) TMA undergoes a ligand-exchange reaction with AlF_3, forms a volatile etch product, and etches Al_2O_3. (b) TMA ligand-exchange with ZrF_4 is unfavorable and results in no etching.

$$Al_2O_3(s) + 6HF(g) \rightarrow 2AlF_3(s) + 3H_2O(g)$$
$$\Delta G^\circ_{285^\circ C} = -50.5 \text{ kcal/mol} \quad (1)$$

$$ZrO_2(s) + 4HF(g) \rightarrow ZrF_4(s) + 2H_2O(g)$$
$$\Delta G^\circ_{285^\circ C} = -13.0 \text{ kcal/mol} \quad (2)$$

The resulting AlF_3 and ZrF_4 surface layers are not volatile. AlF_3 and ZrF_4 sublime at 1276 and 912 °C, respectively.[34]

The following TMA exposure then undergoes a favorable ligand-exchange transmetalation reaction with the AlF_3 surface as illustrated in Figure 6a. During this reaction, CH_3 ligands from TMA exchange with F ligands from the AlF_3 surface. The fundamental reactions proceed as

$$(A1)\ AlF_3(s)^* + Al(CH_3)_3(g) \rightarrow AlF_2CH_3(s)^* + AlF(CH_3)_2(g) \quad (3)$$

$$(A2)\ AlF_2(CH_3)(s)^* + Al(CH_3)_3(g) \rightarrow 2AlF(CH_3)_2(g) \quad (4)$$

where * denotes a surface species.[7] $AlF(CH_3)_2$ (dimethylaluminum fluoride (DMAF)) is the expected product resulting from ligand-exchange from the fluorinated surface to TMA. DMAF is also expected after two ligand-exchange reactions from TMA to AlF_3. DMAF is the observed etch product in recent mass spectrometer studies.[19] However, these mass spectrometry measurements reveal dimers of DMAF with itself (DMAF–DMAF) and with TMA (DMAF–TMA).[19] In addition, trimers are also observed in the mass spectrum.[19]

In contrast, no etching reaction is observed between TMA and the ZrF_4 surface.[24] There is no transfer of methyl ligands between TMA and the ZrF_4 surface as shown in Figure 6b. This lack of methyl transfer is attributed to the unstable Zr–CH_3 bond. To support this explanation, the fully methylated $Zr(CH_3)_4$ species decomposes at temperatures of ≤15 °C.[36] Because no ligand exchange takes place between TMA and ZrF_4, the ZrF_4 film remains intact and blocks the etching of the underlying Al_2O_3 film by sequential HF and TMA exposures.

3.B. Robustness and Performance of ZrO_2 ESL. The robustness of the ZrO_2 ESL was determined by exposing the ZrO_2 ESL to multiple cycles of sequential HF and TMA exposures. Figure 7 shows 100 cycles of sequential HF and

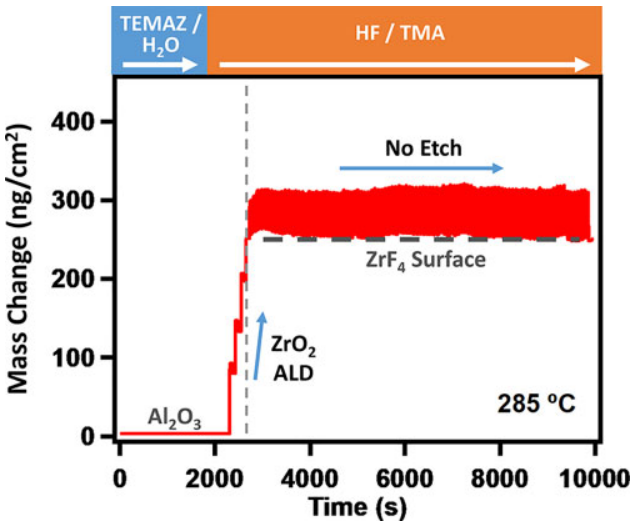

Figure 7. Mass change versus time for ZrO_2ALD using sequential exposures of TEMAZ and H_2O (~250 ng/cm^2 total), followed by 100 sequential exposures of HF and TMA.

TMA exposures on a ZrO_2 ALD film with a coverage of ~200 ng/cm^2 on top of an Al_2O_3 ALD film with a thickness of ~5 nm. The initial exposure to HF fluorinates the ZrO_2 ALD film.[28] Continued cycling causes progressive mass losses with TMA exposures and mass gains with HF exposures. However, there is no net mass change to the fluorinated ZrO_2 ALD film or the underlying Al_2O_3 substrate.

Figure 8 displays the mass changes during the individual HF exposures, ΔM_{HF}, and mass changes during the individual TMA exposures, ΔM_{TMA}, for the 100 cycles of sequential HF and TMA exposures shown in Figure 7. The mass change per

https://dx.doi.org/10.1021/acs.chemmater.0c03335
Chem. Mater. 2020, 32, 10055−10065

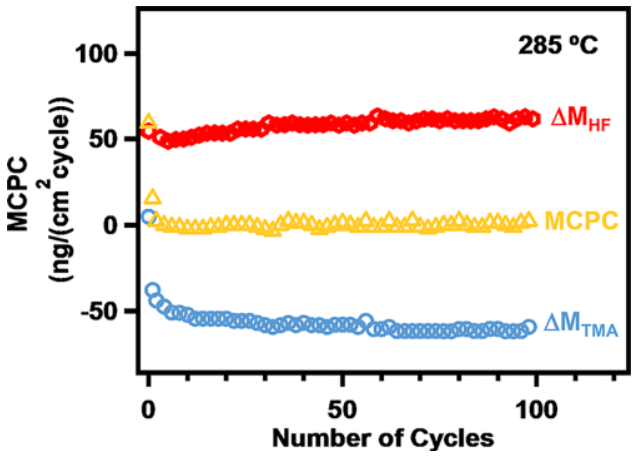

Figure 8. Mass change per cycle for 100 sequential exposures of HF and TMA shown in Figure 7. Results shown for mass change after each HF exposure (ΔM_{HF}), each TMA exposure (ΔM_{TMA}), and total mass change per cycle (MCPC = ΔM_{HF} + ΔM_{TMA}).

cycle, MCPC, is also displayed in Figure 8. The averages are ΔM_{HF} = +61.43 ng/cycle, ΔM_{TMA} = −61.44 ng/cycle, and MCPC = ΔM_{HF} + ΔM_{TMA} ≈ 0 ng/cycle. The negligible MCPC indicates that there is no etching of the film. However, there are mass gains during the HF exposures followed by equal and opposite mass losses during the TMA exposures.

The mass changes versus time for the first few sequential HF and TMA exposures are shown in Figure 9. The first HF pulse

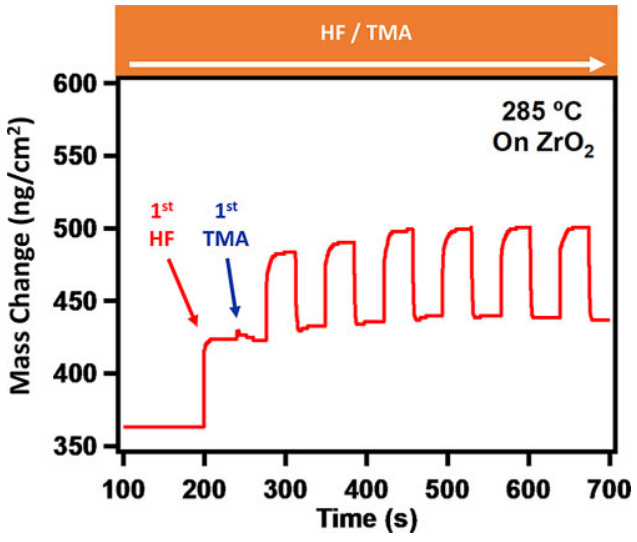

Figure 9. Mass change versus time for first seven cycles of sequential exposures of HF and TMA on ∼1 ML of ZrO_2 ALD on underlying Al_2O_3 ALD film.

results in ΔM_{HF} = +60.3 ng/cm^2 corresponding to the fluorination of the ZrO_2 surface to form a ZrF_4 or ZrO_xF_y surface layer.[28] Assuming that the surface layer is ZrF_4, this mass change corresponds to the fluorination of 8.24 × 10^{14} ZrO_2 units/cm^2 to ZrF_4. This number of ZrO_2 units/cm^2 is close to the expected planar number density of 9.2 × 10^{14} ZrO_2 units/cm^2 that was calculated earlier using a ZrO_2 mass density of 5.68 g/cm^3.

After the first HF exposure, the first TMA exposure in Figure 9 causes a brief mass increase of ∼4 ng/cm^2. This mass increase is quickly lost to yield a net ΔM_{TMA} ≈ 0 ng/cm^2. This short mass fluctuation may be caused by the physical adsorption of TMA molecules on the ZrF_4 surface. These TMA molecules fail to ligand-exchange with the ZrF_4 surface. Consequently, the TMA molecules are free to desorb from the ZrF_4 surface.

Following the first cycle, the subsequent sequential HF and TMA exposures result in mass oscillations of ΔM_{HF} ≈ +61 ng/cm^2 and ΔM_{TMA} ≈ −61 ng/cm^2. The mass increase after HF exposure can be understood by considering the chemical nature of the ZrF_4 surface. The ZrF_4 surface has strong Lewis acid character and is known to adsorb HF.[37] A mass gain of 61 ng/cm^2 during HF exposure is consistent with the adsorption of 1.84 × 10^{15} HF molecules/cm^2 on the ZrF_4 surface.

This quantity of HF molecules adsorbed on the ZrF_4 surface can be compared with earlier studies that examined ZrF_4 ALD using tetrakis(ethylmethylamido)zirconium (TEMAZ) and HF as the reactants at 150 °C.[37] In these earlier *in situ* QCM investigations, HF was concluded to be adsorbed on the ZrF_4 surface following the HF exposures.[37] The HF coverage was quantified in terms of the number of ZrF_4 species deposited during one ZrF_4 ALD cycle. For a ZrF_4 ALD growth rate of 0.9 Å/cycle at 150 °C, there were 2.4 HF molecules adsorbed for every ZrF_4 unit deposited during the ZrF_4 ALD cycle.[37]

A ZrF_4 ALD growth rate of 0.9 Å/cycle is consistent with a ZrF_4 mass gain of 51.1 ng/(cm^2 cycle). This mass gain is equivalent with a ZrF_4 coverage of 1.84 × 10^{14} ZrF_4 units/cm^2. The HF coverage on the ZrF_4 surface at 150 °C is then 1.84 × 10^{14} ZrF_4 units/cm^2 × 2.4 HF/ZrF_4 = 4.4 × 10^{14} HF/cm^2. This HF coverage of 4.4 × 10^{14} HF/cm^2 during ZrF_4 ALD is less than the HF coverage of 1.84 × 10^{15} HF molecules/cm^2 on the surface of the fluorinated ZrO_2 ESL. The HF coverages may be different because the ZrF_4 surfaces are different. During ZrF_4 ALD, the ZrF_4 surface is the surface of a ZrF_4 bulk film. After deposition of one ZrO_2 monolayer, the fluorinated surface is produced by the HF fluorination of one ZrO_2 monolayer on the underlying Al_2O_3 film.

Figure 9 shows that the subsequent TMA exposure causes a mass loss ΔM_{TMA} ≈ −61 ng/cm^2. This mass loss results from the removal of adsorbed HF by the formation of volatile products. This reaction is believed to be

$$ZrF_4|HF^* + Al(CH_3)_3 \rightarrow ZrF_4^* + AlF(CH_3)_2 \quad (5)$$

Mass spectrometer studies are needed to confirm this proposed reaction. After the adsorbed HF is removed by TMA, the TMA cannot ligand-exchange with the ZrF_4 surface. Figure 9 reveals that HF adsorption followed by HF removal by TMA continues indefinitely without etching the surface.

3.C. Removal of ZrO_2 ESL. The ZrO_2 ESL can be removed using a different metal precursor for the ligand-exchange reaction. The ZrO_2 ESL is fluorinated to a ZrF_4 layer by the HF exposure.[28] The ZrF_4 layer does not undergo ligand-exchange with TMA and consequently serves as an ESL for TMA. In contrast, the ZrF_4 will undergo ligand-exchange with $AlCl(CH_3)_2$ (dimethylaluminum chloride (DMAC)).[8] This ligand-exchange is possible because DMAC contains Cl ligands. The Cl ligands can transfer to Zr during ligand-exchange and form stable Zr−Cl bonds.

Zr−Cl bond formation during the reaction between DMAC and ZrF_4 is thermochemically favorable. Ligand-exchange converting ZrF_4 to $ZrCl_4$ could occur based on the reaction ZrF_4 + 4$AlCl(CH_3)_2$ → $ZrCl_4$ + 4$AlF(CH_3)_2$. This ligand-exchange can be modeled using the reaction ZrF_4 +

https://dx.doi.org/10.1021/acs.chemmater.0c03335
Chem. Mater. 2020, 32, 10055−10065

$^4/_3AlCl_3(g) \rightarrow ZrCl_4(g) + {}^4/_3AlF_3$. This model reaction is spontaneous based on a predicted free energy change of $\Delta G = -37$ kcal.[35] In addition, $ZrCl_4$ is stable and volatile.[38]

Figure 10 compares the sequential exposures of HF and TMA and the sequential exposures of HF and DMAC on ZrO_2

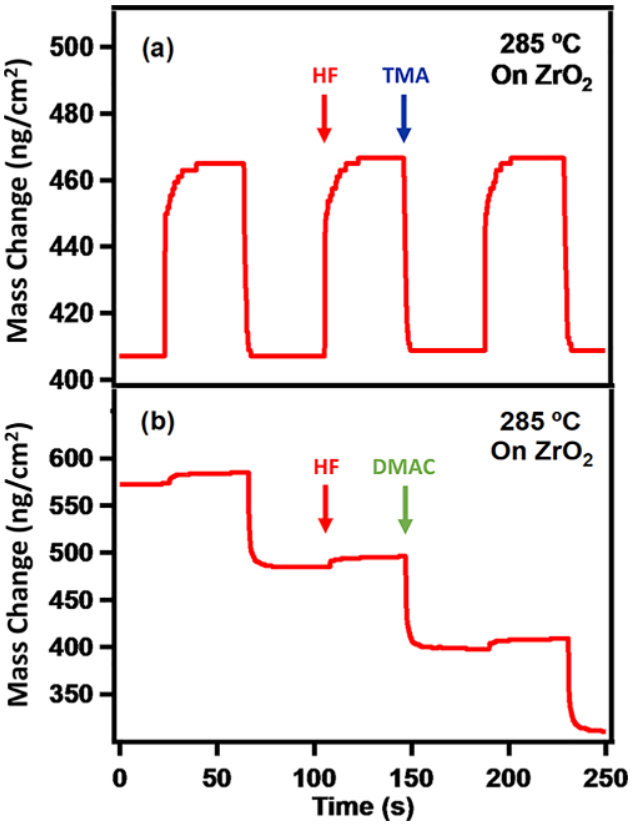

Figure 10. (a) Mass change versus time for sequential exposures of HF and TMA on ZrO_2. (b) Mass change versus time for sequential exposures of HF and DMAC on ZrO_2.

at 285 °C. The mass changes during three cycles of sequential HF and TMA exposures on ZrO_2 are shown in Figure 10a. The mass changes during three cycles of sequential HF and DMAC exposures on ZrO_2 are shown in Figure 10b. The results in Figure 10a are similar to the results in Figure 9. Sequential exposures of HF and TMA repeatedly add mass and remove mass, respectively, with no net etching of the ZrO_2 substrate.

In contrast, sequential HF and DMAC exposures are able to etch ZrO_2.[8,24] Figure 10b shows a mass loss of ~88 ng/(cm^2 cycle) when applying sequential HF and DMAC exposures to ZrO_2. The mass loss is observed when DMAC is able to undergo ligand-exchange with the fluorinated ZrO_2 surface. The ligand-exchange between DMAC and ZrF_4 can produce volatile $ZrCl_xF_y$ etch products. Only a small mass gain is recorded during the HF exposure. The HF exposure is both replacing chlorine ligands and fluorinating ZrO_2. The mass loss from losing chlorine and mass gain from fluorinating ZrO_2 lead to a net mass change of near zero. Similar behavior was observed during HfO_2 ALE using HF and DMAC.[8]

The ability of DMAC to undergo ligand-exchange with the fluorinated ZrO_2 surface is critical to remove the ZrO_2 ESL. Figure 11 illustrates that the ZrO_2 ESL can be deposited on an Al_2O_3 ALD surface using sequential exposures to TEMAZ and

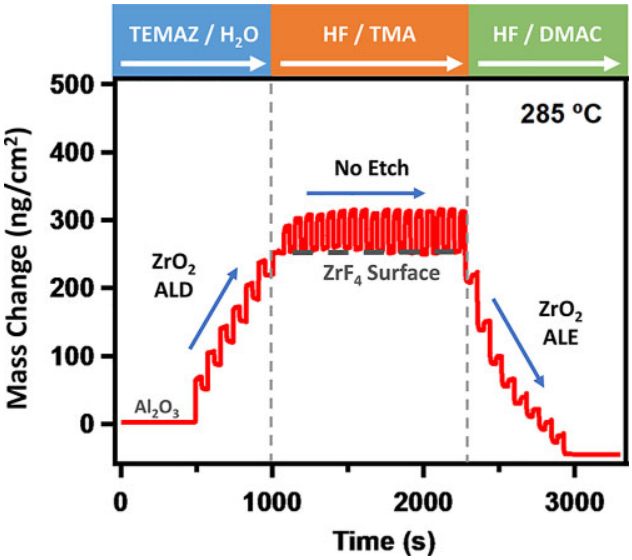

Figure 11. Mass change versus time for ZrO_2 ALD using sequential exposures of TEMAZ and H_2O, followed by sequential exposures of HF and TMA, and last, ZrO_2 ALE using sequential exposures of HF and DMAC.

H_2O. Subsequently, the ZrO_2 ESL blocks Al_2O_3 ALE using sequential HF and TMA exposures. After blocking Al_2O_3 ALE, the ZrO_2 ESL can be removed using sequential HF and DMAC exposures. Figure 11 shows that all of these processes can be conducted effectively and quickly at 285 °C. The ZrO_2 ESL can be deposited and removed repeatedly with no change in the Al_2O_3 etching rate after removal of the ZrO_2 ESL.

The sequential HF and DMAC exposures will etch both ZrO_2 and Al_2O_3.[8,24] Consequently, after the sequential HF and DMAC exposures remove the ZrO_2 ESL, the sequential exposures continue to etch the underlying Al_2O_3 substrate. Figure 12 displays the mass change versus time for sequential HF and DMAC exposures on a ZrO_2 layer on an Al_2O_3 film.

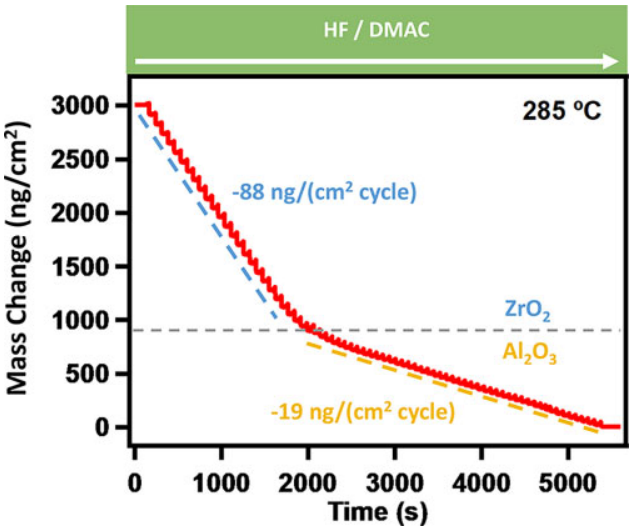

Figure 12. Mass change versus time for sequential exposures of HF and DMAC on ZrO_2 ALD film on top of Al_2O_3 ALD film. Dashed gray line represents interface between ZrO_2 ALD film and Al_2O_3 ALD film.

https://dx.doi.org/10.1021/acs.chemmater.0c03335
Chem. Mater. 2020, 32, 10055−10065

The initial cycles show ZrO_2 ALE in steady state with an etch rate of 88 ng/(cm^2 cycle). The etch rate slows approaching the interface between the ZrO_2 layer and the underlying Al_2O_3 film. After a short transition region, the Al_2O_3 ALE occurs at an etch rate of 19 ng/(cm^2 cycle) using sequential HF and DMAC exposures.

Etch stop layers are frequently incorporated within stacks of materials and act to stop a particular etch process at a desired interface.[25] A buried ZrO_2 ESL can be used to stop etching using sequential HF and TMA exposures. Figure 13 displays

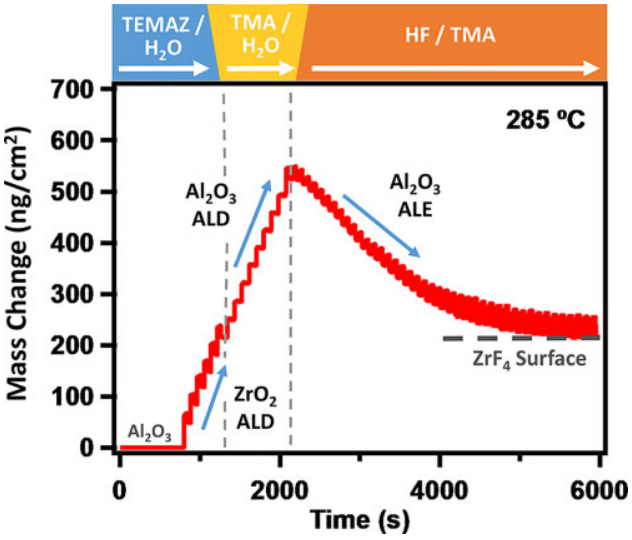

Figure 13. Mass change versus time for ZrO_2 ALD using sequential exposures of TEMAZ and H_2O on Al_2O_3 substrate, followed by Al_2O_3 ALD using sequential exposures of TMA and H_2O, and last, Al_2O_3 ALE using sequential exposures of HF and TMA. ZrO_2 ALD film serves as etch stop for Al_2O_3 ALE.

mass change versus time for Al_2O_3 ALE using sequential HF and TMA exposures. Prior to the Al_2O_3 ALE, a ZrO_2 ESL with ~200 ng/cm^2 of ZrO_2 was deposited and then buried under an Al_2O_3 ALD layer with ~340 ng/cm^2 of Al_2O_3. The Al_2O_3 etching rate begins to slow approaching the Al_2O_3/ZrO_2 interface. After the HF fluorination of the ZrO_2 surface, the ZrO_2 ESL prevents any further etching because the TMA cannot undergo ligand-exchange with the fluorinated ZrO_2 surface.

3.D. *Ex Situ* Spectroscopic Ellipsometry and XPS Measurements. The ZrO_2 monolayer ESL was also deposited on Al_2O_3 ALD layers on Si wafers. The thickness of the Al_2O_3 ALD layer with and without the ZrO_2 monolayer ESL was then monitored using *ex situ* spectroscopic ellipsometry. Figure 14 displays the Al_2O_3 film thickness versus number of sequential HF and TMA exposures for the Al_2O_3 film protected with the ZrO_2 ESL and the Al_2O_3 film without the ZrO_2 ESL. The Al_2O_3 film without the ZrO_2 ESL is etched at a constant etch rate of 0.42 Å/cycle. In contrast, the film protected by a ZrO_2 monolayer ESL exhibits no etching over the 100 cycles of sequential HF and TMA exposures.

Ex situ X-ray photoelectron (XPS) spectroscopy was used to confirm that the ZrO_2 ESL could be removed from the Al_2O_3 film. Two individual samples were prepared on Si wafers by growing a ZrO_2 monolayer ESL on top of an Al_2O_3 ALD film. Subsequently, one sample was subjected to 10 cycles of

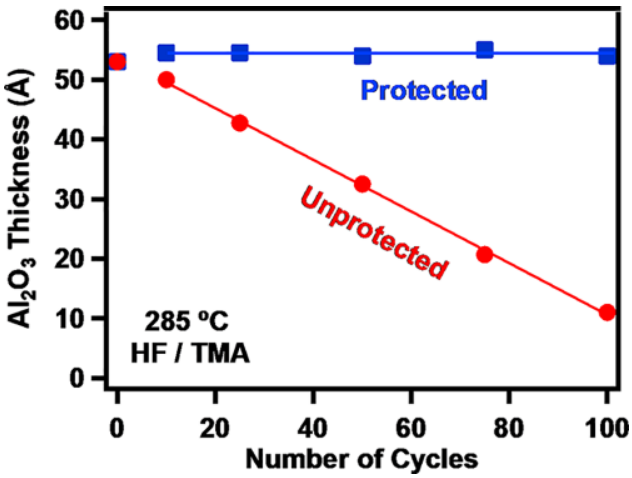

Figure 14. Spectroscopic ellipsometry measurements of Al_2O_3 film thickness versus number of sequential exposures of HF and TMA on an Al_2O_3 ALD film (unprotected) and an Al_2O_3 ALD film coated with ~1 ML ZrO_2 ALD (protected).

sequential HF and TMA exposures at 285 °C. The other sample was subjected to 10 cycles of sequential HF and DMAC exposures at 285 °C. The XPS spectra after these sequential exposures are shown in Figure 15.

The XPS spectra in Figure 15a confirms the presence of Zr on the Al_2O_3 film exposed to 10 sequential cycles of HF and TMA. Zr is identified by the prominent Zr 3s, Zr 3p, and Zr 3d XPS peaks. These results indicate that the ZrO_2 monolayer ESL is not removed by sequential HF and TMA exposures. In

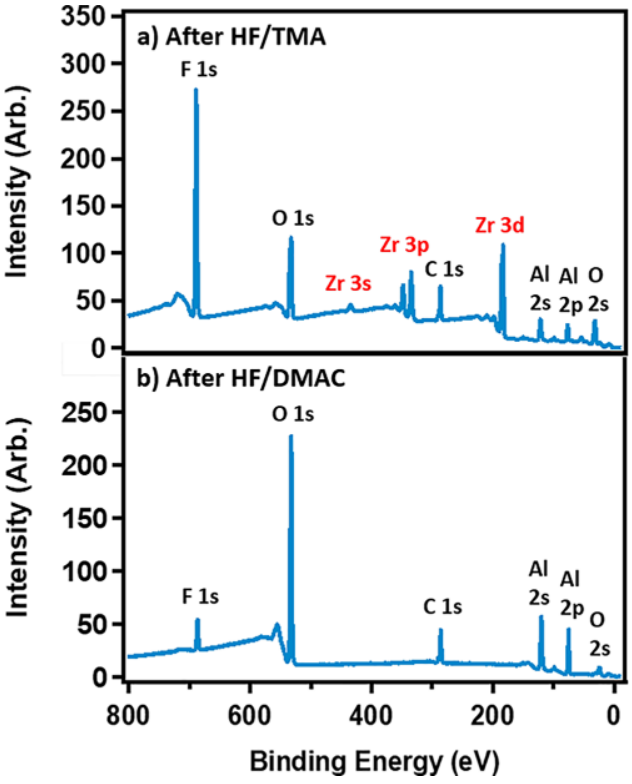

Figure 15. XPS spectra for a ZrO_2 monolayer ESL on an Al_2O_3 ALD film exposed to (a) 10 cycles of HF/TMA and (b) 10 cycles of HF/DMAC.

https://dx.doi.org/10.1021/acs.chemmater.0c03335
Chem. Mater. 2020, 32, 10055−10065

contrast, Figure 15b demonstrates that there was no Zr on the Al_2O_3 film exposed to 10 sequential cycles of HF and DMAC. The ZrO_2 monolayer ESL is easily removed by sequential HF and DMAC exposures. Additional experiments determined that no measurable Zr XPS signals were present after 7−8 cycles of sequential HF and DMAC exposures.

3.E. Monolayer ESL for Selective Thermal ALE. The monolayer ESL will be useful for selective thermal ALE if the monolayer ESL can be deposited selectively on different materials. The selective deposition of the ZrO_2 monolayer ESL is equivalent to area selective ZrO_2 ALD. In the field of area selective ALD, the selective deposition can result from nucleation differences between various materials. Examples of area selective ALD based on nucleation delays include W ALD on Si−H on silicon surfaces in preference to SiO_2 surfaces[39] and Co ALD on metal surfaces rather than silicon surfaces.[40]

Area selective ALD can also occur based on a combination of ALD and etching. Nucleation differences may initially favor ALD on one "growth" substrate rather than another "nongrowth" substrate. However, eventually the ALD begins to occur on the "nongrowth" substrate. Etching can be employed to remove the nucleation islands from the "nongrowth" substrate. Although the etching process does remove some of the ALD from the "growth" substrate, the selectivity of the ALD on the "growth" substrate is very high with no deposition on the "nongrowth" substrate. Examples of this area selective ALD include Ta_2O_5 and TiO_2 plasma-enhanced ALD (PE-ALD) on TiN surfaces in preference to Si or SiO_2 surfaces,[41,42] TiO_2 ALD on SiO_2 surfaces rather than Si−H surfaces,[43] and Ru ALD on Pt surfaces preferably to SiO_2 surfaces.[44]

In addition, area selective deposition can result from using surface blocking agents such as self-assembled monolayers (SAMs) to mask particular materials. Examples of area selective ALD based on masking with SAMs include HfO_2 ALD on silicon surfaces in preference to SiO_2 surfaces[45] and ZnO ALD on SiO_2 surfaces rather than various metal surfaces.[46] Other schemes for area selective deposition are based on inhibitor or blocking molecules. Examples of area selective ALD using inhibitor molecules include Pt ALD on Si surfaces in preference to SiO_2 surfaces inhibited with diethylamino trimethylsilane[47] and SiO_2 ALD on SiO_2 or SiN_x surfaces rather than Al_2O_3, TiO_2, or HfO_2 surfaces inhibited with acetylacetone.[48]

By use of the area-selective deposition of monolayer ESLs, area-selective thermal ALE could be achieved between various materials. This additional selectivity could complement the inherent selectivity in thermal ALE. This intrinsic selectivity results primarily from the ligand-exchange reaction.[24] Only ligand-exchange reactions that yield stable and volatile products will lead to etching.[24] The inherent selectivity is also derived from the thermochemistry of the surface reactions.[10,24] The area-selective deposition of monolayer ESLs will add new etch blocking possibilities and increase the potential applications for selective thermal ALE.

4. CONCLUSIONS

ZrO_2 thin films were demonstrated as an etch stop layer (ESL) for the thermal ALE of Al_2O_3 using sequential exposures of HF and TMA at 285 °C. *In situ* quartz crystal microbalance (QCM) measurements determined that the ZrO_2 ESL was effective at completely inhibiting Al_2O_3 ALE when the mass of the deposited ZrO_2 film was ≥190 ng/cm^2. The minimum effective mass is approximately the mass of one ZrO_2 monolayer and is equivalent to a ZrO_2 thickness of 3.3 Å. When the mass of deposited ZrO_2 was below the mass of one ZrO_2 monolayer, the underlying Al_2O_3 etch rates were proportional to ZrO_2 fractional coverage.

The ZrO_2 ESL was deposited on Al_2O_3 using tetrakis-(ethylmethylamido)zirconium (TEMAZ) and H_2O. The ZrO_2 ESL was effective for hundreds of thermal Al_2O_3 ALE cycles. The ZrO_2 ESL could be removed when desired by ZrO_2 ALE using HF and dimethylaluminum chloride (DMAC). X-ray photoelectron spectroscopy (XPS) studies observed no trace of Zr on the Al_2O_3 surface after 7−8 cycles of HF and DMAC sequential exposures. The ZrO_2 ESL could be deposited and removed repeatedly without changing the Al_2O_3 etch rate.

The ZrO_2 ESL was also effective when buried in a material stack. When one ZrO_2 monolayer was grown in layers of Al_2O_3, the sequential exposures of HF and TMA etched the top layer of Al_2O_3. The etching came to a halt where the ZrO_2 film was buried and the ZrO_2 film inhibited the etching of the underlying Al_2O_3 layer. The ZrO_2 monolayer etch stop concept is general and should be extendable to other materials. Monolayer ESLs could serve as a valuable processing tool to block etching for fabrication of complex semiconductor stacks and advanced nanoscale architectures.

AUTHOR INFORMATION

Corresponding Author

Steven M. George − *Department of Chemistry, University of Colorado, Boulder, Colorado 80309, United States;* orcid.org/0000-0003-0253-9184; Email: steven.george@colorado.edu

Authors

David R. Zywotko − *Department of Chemistry, University of Colorado, Boulder, Colorado 80309, United States*

Omid Zandi − *Tokyo Electron America, Inc., Austin, Texas 78741, United States*

Jacques Faguet − *Tokyo Electron America, Inc., Austin, Texas 78741, United States*

Paul R. Abel − *Tokyo Electron America, Inc., Austin, Texas 78741, United States*

Complete contact information is available at: https://pubs.acs.org/10.1021/acs.chemmater.0c03335

Notes

The authors declare no competing financial interest.

ACKNOWLEDGMENTS

This research was funded by Tokyo Electron Limited. The authors thank Dr. Andrew Cavanagh for providing the XPS elemental analysis.

REFERENCES

(1) George, S. M. Atomic Layer Deposition: An Overview. *Chem. Rev.* **2010**, *110*, 111−131.

(2) Kanarik, K. J.; Lill, T.; Hudson, E. A.; Sriraman, S.; Tan, S.; Marks, J.; Vahedi, V.; Gottscho, R. A. Overview of Atomic Layer Etching in the Semiconductor Industry. *J. Vac. Sci. Technol., A* **2015**, *33*, 020802.

(3) Lee, Y.; George, S. M. Atomic Layer Etching of Al_2O_3 Using Sequential, Self-Limiting Thermal Reactions with $Sn(acac)_2$ and HF. *ACS Nano* **2015**, *9*, 2061−2070.

(4) George, S. M. Mechanisms of Thermal Atomic Layer Etching. *Acc. Chem. Res.* **2020**, *53*, 1151−1160.

(5) Oehrlein, G. S.; Metzler, D.; Li, C. Atomic Layer Etching at the Tipping Point: An Overview. *ECS J. Solid State Sci. Technol.* **2015**, *4*, N5041−N5053.
(6) George, S. M.; Lee, Y. Prospects for Thermal Atomic Layer Etching Using Sequential, Self-Limiting Fluorination and Ligand-Exchange Reactions. *ACS Nano* **2016**, *10*, 4889−4894.
(7) Lee, Y.; DuMont, J. W.; George, S. M. Trimethylaluminum as the Metal Precursor for the Atomic Layer Etching of Al_2O_3 Using Sequential, Self-Limiting Thermal Reactions. *Chem. Mater.* **2016**, *28*, 2994−3003.
(8) Lee, Y.; George, S. M. Thermal Atomic Layer Etching of Al_2O_3, HfO_2, and ZrO_2 Using Sequential Hydrogen Fluoride and Dimethylaluminum Chloride Exposures. *J. Phys. Chem. C* **2019**, *123*, 18455−18466.
(9) Lee, Y.; DuMont, J. W.; George, S. M. Atomic Layer Etching of HfO_2 Using Sequential, Self-Limiting Thermal Reactions with $Sn(acac)_2$ and HF. *ECS J. Solid State Sci. Technol.* **2015**, *4*, N5013−N5022.
(10) Lee, Y.; George, S. M. Thermal Atomic Layer Etching of HfO_2 Using HF for Fluorination and $TiCl_4$ for Ligand-Exchange. *J. Vac. Sci. Technol., A* **2018**, *36*, 061504.
(11) Zywotko, D. R.; George, S. M. Thermal Atomic Layer Etching of ZnO by a "Conversion-Etch" Mechanism Using Sequential Exposures of Hydrogen Fluoride and Trimethylaluminum. *Chem. Mater.* **2017**, *29*, 1183−1191.
(12) Lee, Y.; George, S. M. Thermal Atomic Layer Etching of Titanium Nitride Using Sequential, Self-Limiting Reactions: Oxidation to TiO_2 and Fluorination to Volatile TiF_4. *Chem. Mater.* **2017**, *29*, 8202−8210.
(13) Johnson, N. R.; George, S. M. WO_3 and W Thermal Atomic Layer Etching Using "Conversion-Fluorination" and "Oxidation-Conversion-Fluorination" Mechanisms. *ACS Appl. Mater. Interfaces* **2017**, *9*, 34435−34447.
(14) Abdulagatov, A. I.; George, S. M. Thermal Atomic Layer Etching of Silicon Using O_2, HF, and $Al(CH_3)_3$ as the Reactants. *Chem. Mater.* **2018**, *30*, 8465−8475.
(15) DuMont, J. W.; Marquardt, A. E.; Cano, A. M.; George, S. M. Thermal Atomic Layer Etching of SiO_2 by a "Conversion-Etch" Mechanism Using Sequential Reactions of Trimethylaluminum and Hydrogen Fluoride. *ACS Appl. Mater. Interfaces* **2017**, *9*, 10296−10307.
(16) Abdulagatov, A. I.; George, S. M. Thermal Atomic Layer Etching of Silicon Nitride Using an Oxidation and "Conversion Etch" Mechanism. *J. Vac. Sci. Technol., A* **2020**, *38*, 022607.
(17) Cano, A. M.; Marquardt, A. E.; DuMont, J. W.; George, S. M. Effect of HF Pressure on Thermal Al_2O_3 Atomic Layer Etch Rates and Al_2O_3 Fluorination. *J. Phys. Chem. C* **2019**, *123*, 10346−10355.
(18) Natarajan, S. K.; Elliott, S. D. Modeling the Chemical Mechanism of the Thermal Atomic Layer Etch of Aluminum Oxide: A Density Functional Theory Study of Reactions during HF Exposure. *Chem. Mater.* **2018**, *30*, 5912−5922.
(19) Clancey, J. W.; Cavanagh, A. S.; Smith, J. E. T.; Sharma, S.; George, S. M. Volatile Etch Species Produced During Thermal Al_2O_3 Atomic Layer Etching. *J. Phys. Chem. C* **2020**, *124*, 287−299.
(20) Osakada, K. Transmetalation. In *Fundamentals of Molecular Catalysis*; Kurosawa, H., Yamamoto, A.. Eds.; Current Methods in Inorganic Chemistry, Vol. 3; Elsevier Science: Amsterdam, 2003; pp 233−291.
(21) King, S. W. Dielectric Barrier, Etch Stop, and Metal Capping Materials for State of the Art and beyond Metal Interconnects. *ECS J. Solid State Sci. Technol.* **2015**, *4*, N3029−N3047.
(22) Mackus, A. J. M.; Merkx, M. J. M.; Kessels, W. M. M. From the Bottom-Up: Toward Area-Selective Atomic Layer Deposition with High Selectivity. *Chem. Mater.* **2019**, *31*, 2−12.
(23) Carver, C. T.; Plombon, J. J.; Romero, P. E.; Suri, S.; Tronic, T. A.; Turkot, R. B. Atomic Layer Etching: An Industry Perspective. *ECS J. Solid State Sci. Technol.* **2015**, *4*, N5005−N5009.
(24) Lee, Y.; Huffman, C.; George, S. M. Selectivity in Thermal Atomic Layer Etching Using Sequential, Self-Limiting Fluorination and Ligand-Exchange Reactions. *Chem. Mater.* **2016**, *28*, 7657−7665.
(25) Collins, S. D. Etch stop techniques for micromachining. *J. Electrochem. Soc.* **1997**, *144*, 2242−2262.
(26) Westerman, R.; Johnson, D.; Lai, S. L.; Teixeira, M. Endpoint detection methods for time division multiplex etch processes. In *Micromachining and Microfabrication Process Technology Xi*; Maher, M. A., Stewart, H. D., Chiao, J. C., Eds.; Proceedings of SPIE, 6109; SPIE, 2006.
(27) Peercy, P. S. The drive to miniaturization. *Nature* **2000**, *406*, 1023−1026.
(28) Mullins, R.; Natarajan, S. K.; Elliott, S. D.; Nolan, M. Self-Limiting Temperature Window for Thermal Atomic Layer Etching of HfO_2 and ZrO_2 Based on the Atomic-Scale Mechanism. *Chem. Mater.* **2020**, *32*, 3414−3426.
(29) Elam, J. W.; Groner, M. D.; George, S. M. Viscous flow reactor with quartz crystal microbalance for thin film growth by atomic layer deposition. *Rev. Sci. Instrum.* **2002**, *73*, 2981−2987.
(30) Rocklein, M. N.; George, S. M. Temperature-Induced Apparent Mass Changes Observed During Quartz Crystal Microbalance Measurements of Atomic Layer Deposition. *Anal. Chem.* **2003**, *75*, 4975−4982.
(31) Hausmann, D. M.; Kim, E.; Becker, J.; Gordon, R. G. Atomic Layer Deposition of Hafnium and Zirconium Oxides Using Metal Amide Precursors. *Chem. Mater.* **2002**, *14*, 4350−4358.
(32) Ott, A. W.; Klaus, J. W.; Johnson, J. M.; George, S. M. Al_2O_3 Thin Film Growth on Si(100) Using Binary Reaction Sequence Chemistry. *Thin Solid Films* **1997**, *292*, 135−144.
(33) Lee, Y.; DuMont, J. W.; Cavanagh, A. S.; George, S. M. Atomic Layer Deposition of AlF_3 Using Trimethylaluminum and Hydrogen Fluoride. *J. Phys. Chem. C* **2015**, *119*, 14185−14194.
(34) *CRC Handbook of Chemistry and Physics*; CRC Press: Boca Raton, FL.
(35) *HSC Chemistry; HSC Chemistry 5.1*; Outokumpu Research Oy: Pori, Finland.
(36) Berthold, H. J.; Groh, G. Preparation of Tetramethylzirconium, $Zr(CH_3)_4$. *Angew. Chem., Int. Ed. Engl.* **1966**, *5*, 516.
(37) Lee, Y.; Sun, H. X.; Young, M. J.; George, S. M. Atomic Layer Deposition of Metal Fluorides Using HF-Pyridine as the Fluorine Precursor. *Chem. Mater.* **2016**, *28*, 2022−2032.
(38) Palko, A. A.; Ryon, A. D.; Kuhn, D. W. The Vapor Pressures of Zirconium Tetrachloride and Hafnium Tetrachloride. *J. Phys. Chem.* **1958**, *62*, 319−322.
(39) Kalanyan, B.; Lemaire, P. C.; Atanasov, S. E.; Ritz, M. J.; Parsons, G. N. Using Hydrogen To Expand the Inherent Substrate Selectivity Window During Tungsten Atomic Layer Deposition. *Chem. Mater.* **2016**, *28*, 117−126.
(40) Kerrigan, M. M.; Klesko, J. P.; Rupich, S. M.; Dezelah, C. L.; Kanjolia, R. K.; Chabal, Y. J.; Winter, C. H. Substrate Selectivity in the Low Temperature Atomic Layer Deposition of Cobalt Metal Films from bis(1,4-di-tert-butyl-1,3-diazadienyl) cobalt and Formic Acid. *J. Chem. Phys.* **2017**, *146*, 052813.
(41) Vallat, R.; Gassilloud, R.; Eychenne, B.; Vallee, C. Selective Deposition of Ta_2O_5 by Adding Plasma Etching Super-Cycles in Plasma Enhanced Atomic Layer Deposition Steps. *J. Vac. Sci. Technol., A* **2017**, *35*, 01b104.
(42) Vallat, R.; Gassilloud, R.; Salicio, O.; El Hajjam, K.; Molas, G.; Pelissier, B.; Vallee, C. Area Selective Deposition of TiO_2 by Intercalation of Plasma Etching Cycles in PEALD Process: A Bottom Up Approach for the Simplification of 3D Integration Scheme. *J. Vac. Sci. Technol., A* **2019**, *37*, 020918.
(43) Song, S. K.; Saare, H.; Parsons, G. N. Integrated Isothermal Atomic Layer Deposition/Atomic Layer Etching Supercycles for Area-Selective Deposition of TiO_2. *Chem. Mater.* **2019**, *31*, 4793−4804.
(44) Vos, M. F. J.; Chopra, S. N.; Verheijen, M. A.; Ekerdt, J. G.; Agarwal, S.; Kessels, W. M. M.; Mackus, A. J. M. Area-Selective Deposition of Ruthenium by Combining Atomic Layer Deposition and Selective Etching. *Chem. Mater.* **2019**, *31*, 3878−3882.

https://dx.doi.org/10.1021/acs.chemmater.0c03335
Chem. Mater. 2020, 32, 10055−10065

(45) Chen, R.; Bent, S. F. Chemistry for Positive Pattern Transfer Using Area-Selective Atomic Layer Deposition. *Adv. Mater.* **2006**, *18*, 1086−1090.
(46) Bobb-Semple, D.; Nardi, K. L.; Draeger, N.; Hausmann, D. M.; Bent, S. F. Area-Selective Atomic Layer Deposition Assisted by Self-Assembled Monolayers: A Comparison of Cu, Co, W, and Ru. *Chem. Mater.* **2019**, *31*, 1635−1645.
(47) Khan, R.; Shong, B.; Ko, B. G.; Lee, J. K.; Lee, H.; Park, J. Y.; Oh, I. K.; Raya, S. S.; Hong, H. M.; Chung, K. B.; Luber, E. J.; Kim, Y. S.; Lee, C. H.; Kim, W. H.; Lee, H. B. R. Area-Selective Atomic Layer Deposition Using Si Precursors as Inhibitors. *Chem. Mater.* **2018**, *30*, 7603−7610.
(48) Mameli, A.; Merkx, M. J. M.; Karasulu, B.; Roozeboom, F.; Kessels, W. M. M.; Mackus, A. J. M. Area-Selective Atomic Layer Deposition of SiO_2 Using Acetylacetone as a Chemoselective Inhibitor in an ABC-Type Cycle. *ACS Nano* **2017**, *11*, 9303−9311.

https://dx.doi.org/10.1021/acs.chemmater.0c03335
Chem. Mater. 2020, 32, 10055−10065